npj | 2D materials and applications

www.nature.com/npj2dmaterials

ARTICLE OPEN

Check for updates

Anomalous conductance quantization of a one-dimensional channel in monolayer WSe_2

Justin Boddison-Chouinard[1,2], Alex Bogan[2], Pedro Barrios[3], Jean Lapointe[3], Kenji Watanabe[4], Takashi Taniguchi[5], Jarosław Pawłowski[6], Daniel Miravet[1], Maciej Bieniek[6,7], Pawel Hawrylak[1], Adina Luican-Mayer[1]✉ and Louis Gaudreau[2]✉

Among quantum devices based on 2D materials, gate-defined quantum confined 1D channels are much less explored, especially in the high-mobility regime where many-body interactions play an important role. We present the results of measurements and theory of conductance quantization in a gate-defined one-dimensional channel in a single layer of transition metal dichalcogenide material WSe_2. In the quasi-ballistic regime of our high-mobility sample, we report conductance quantization steps in units of e^2/h for a wide range of carrier concentrations. Magnetic field measurements show that as the field is raised, higher conductance plateaus move to accurate quantized values and then shift to lower conductance values while the e^2/h plateau remains locked. Based on microscopic atomistic tight-binding theory, we show that in this material, valley and spin degeneracies result in 2 e^2/h conductance steps for noninteracting holes, suggesting that symmetry-breaking mechanisms such as valley polarization dominate the transport properties of such quantum structures.

npj 2D Materials and Applications (2023)7:50 ; https://doi.org/10.1038/s41699-023-00407-y

INTRODUCTION

Realization of quantum devices based on two-dimensional (2D) materials has attracted significant interest in recent years[1,2]; in particular, advances in fabrication techniques for devices based on transition metal dichalcogenides (TMDs) enabled the realization of building blocks of quantum circuits such as gate-controlled quantum dots in monolayer and few-layer MoS_2[3–6] and WSe_2[7,8] as well as one-dimensional (1D) channels based on split gate technology[9–13]. 1D channels are of great interest in quantum information science because they have been established as valuable tools for noninvasive readout of semiconducting charge and spin qubits in GaAs[14], SiGe[15], graphene[16–19], bilayer graphene[20,21], and WSe_2[22]. In 1D channels, the Landauer–Buttiker formalism explains the quantized conductance in units of $n\ e^2/h$, where n is the number of available transport channels, which depends on the degeneracies of the system; for example, twofold spin degeneracy for GaAs[23] and fourfold spin and valley degeneracy for graphene[24]. Beyond this picture, much less is known about the mechanisms through which interaction effects can add complexity and play a role in transport anomalies[23]. Therefore, 1D channels based on high-mobility 2D materials offer the possibility to access interaction regimes.

Here, we present results of investigation of a 1D channel based on high-mobility monolayer WSe_2, and find that the conductance is quantized in units of e^2/h. This is surprising since in monolayer TMDs, due to spin-valley locking, we expect conductance quantization for noninteracting holes in units of 2 e^2/h. Our results are in agreement with reports using few-layer MoS_2[9,11], trilayer WSe_2[13] and monolayer MoS_2[10], but the origin of the e^2/h quantization remains unexplained. We attribute this broken valley and spin degeneracy to the formation of valley and spin-polarized states of holes, which have been predicted for WS_2[25,26] and in laterally gated MoS_2 quantum dots[27,28].

Although there is already a substantial body of work explaining non-universal conductance quantization, a full understanding of the so-called "0.7 anomaly" in quantum point contacts remains elusive and is assumed to be due to electron–electron interactions[29–38]. While the full theory of conductance in the presence of hole–hole interactions is in progress, here we show a complete single-particle model based on atomistic tight-binding theory for holes in a WSe_2 monolayer, confined in an electrostatically defined 1D channel. It demonstrates that a channel potential does not break valley degeneracy and without hole–hole interactions conductance is expected to be quantized in units of 2 e^2/h. Hence the observed anomalous quantization in units of e^2/h can likely be explained in terms of broken symmetry valley-polarized ground state induced by interactions[25,26,39].

RESULTS

Device structure

Using standard dry transfer methods[40,41], a van der Waals heterostructure consisting of a monolayer WSe_2 flake encapsulated between two hexagonal boron nitride (hBN) flakes was assembled on a p-doped silicon substrate with 285 nm of thermally grown silicon dioxide (SiO_2). The silicon substrate was utilized as a back gate to introduce carriers in the WSe_2 layer. Electron beam lithography was used to define electrical contacts [Cr (2 nm)/Pt (8 nm)][42], which contact the WSe_2 from the bottom, and to pattern a 4-component top gate. Two of the top gates, labeled as V_{CG} in Fig. 1a, cover the area where there is overlap between the WSe_2 flake and the electrical contacts, and are used to activate the electrical contacts. The two other top gates, labeled

[1]Department of Physics, University of Ottawa, Ottawa, ON K1N 9A7, Canada. [2]Emerging Technologies Division, National Research Council of Canada, Ottawa, ON K1A 0R6, Canada. [3]Advanced Electronics and Photonics, National Research Council of Canada, Ottawa, ON K1A 0R6, Canada. [4]Research Center for Functional Materials, National Institute for Materials Science, 1-1 Namiki, Tsukuba 305-0044, Japan. [5]International Center for Materials Nanoarchitectonics, National Institute for Materials Science, 1-1 Namiki, Tsukuba 305-0044, Japan. [6]Institute of Theoretical Physics, Wrocław University of Science and Technology, Wrocław, Poland. [7]Institute of Theoretical Physics, Würzburg University, Würzburg, Germany. ✉email: luican-mayer@uottawa.ca; louis.gaudreau@nrc-cnrc.gc.ca

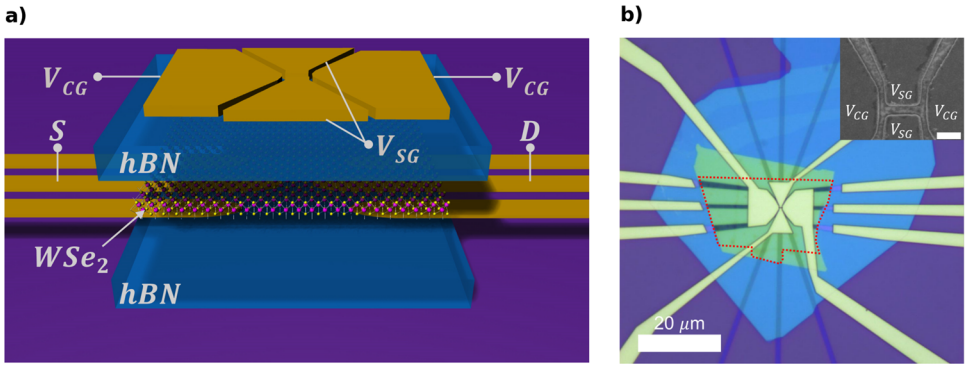

Fig. 1 Monolayer WSe_2 device structure. a Schematic of the monolayer WSe_2 device structure. **b** Optical micrograph of the device used in this study. The WSe_2 monolayer flake is outlined in red for clarity. Inset: Scanning electron micrograph of the top gate structure (scalebar is 400 nm). The left and right gates are used to activate the contact region (V_{CG}). The top and bottom gates (V_{SG}) are used to form the 1D channel. The 1D channel is lithographically defined to have a width of 200 nm and a length of 600 nm.

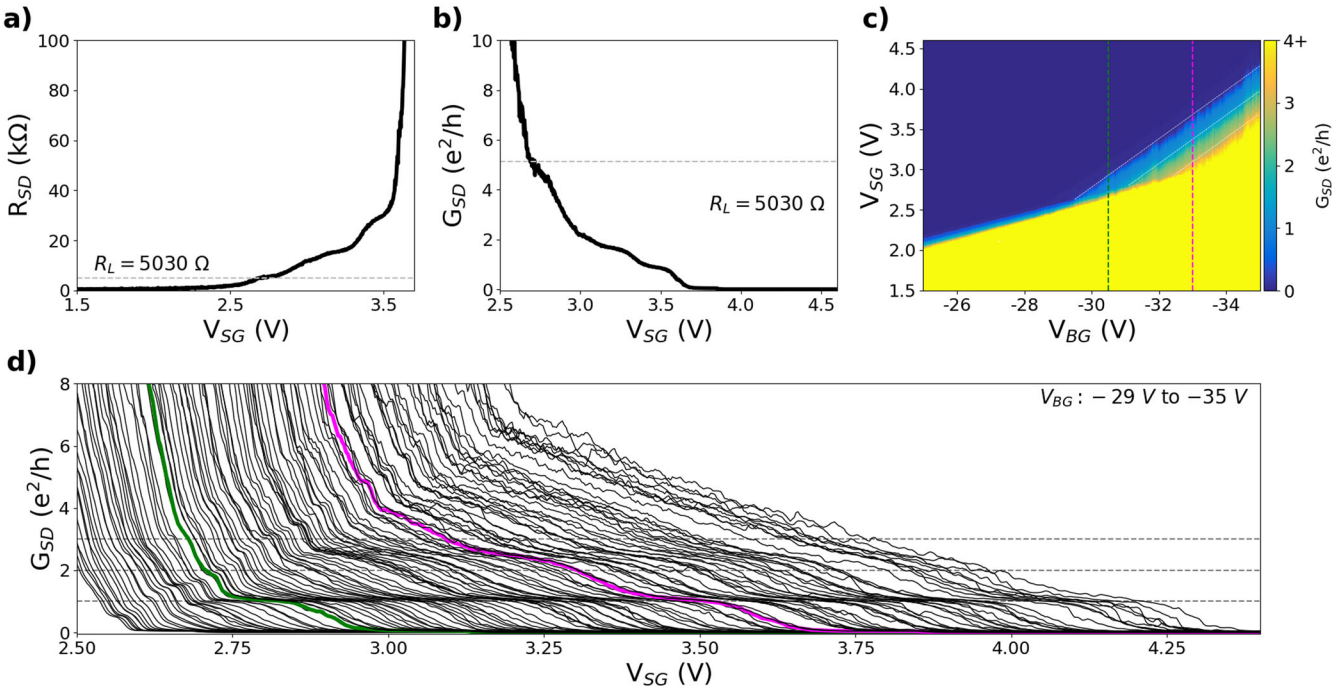

Fig. 2 Formation of a 1D channel and its dependence on the hole concentration. a 4-point measurement of resistance vs. split gate voltage (V_{SG}) at $V_{BG} = -33$ V. The dashed line indicates the resistance where the channel is formed (at depletion). **b** Conductance in units of e^2/h vs. split gate voltage (V_{SG}) at $V_{BG} = -33$ V. The dashed line represents the conductance where the channel is formed (at depletion). **c** Color map of conductance as a function of split gate voltage V_{SG} and back gate voltage V_{BG}. A lead resistance (resistance at depletion) is subtracted. **d** Line cuts from (**c**) plotted in a "waterfall" style indicating a first step at e^2/h and a second step around 2 e^2/h. The leftmost trace is taken at $V_{BG} = -29$ V and the right most trace is taken at $V_{BG} = -35$ V. The green and magenta lines are highlighted by similarly colored dashed lines in (**c**) and correspond to back gate voltages of −30.5 V and −33 V, respectively. These two curves feature the regimes where we observe the 1 e^2/h plateau (green), and the 1 e^2/h and 2 e^2/h plateaus (magenta).

as V_{SG} in Fig. 1a, were used to define the 1D channel in the WSe_2 with a lithographic width of 200 nm and length of 600 nm as confirmed by a scanning electron micrograph (Fig. 1b, inset). Many important cleaning techniques were employed throughout the fabrication procedure and are detailed in "Methods". Figure 1b shows an optical micrograph of the completed device.

Electrical transport in a WSe_2 1D channel

We first demonstrate that we can create a conduction region with a sufficiently low resistance to study quantized conductance at a temperature of 4 K. Figure 2a is a 4-point measurement of the device resistance R_{SD} as a function of the split gate voltage V_{SG} at a constant source-drain current of 10 nA and constant back gate voltage $V_{BG} = -33$ V. At low V_{SG}, when the voltages on the split gate are not sufficiently high to deplete the underlying WSe_2 regions from carriers, we measure a resistance of 480 Ω from which we are able to extract a contact resistance of 9.76 kΩ (see Supplementary Fig. 1), a value that is comparable to others reported using more complex fabrication techniques[13,43,44]. As the voltage is increased on the split gates, we observe an increase in resistance, indicating that a constriction has been formed and that holes are responsible for transport in the device.

The change in the conductance of the device in units of e^2/h as a function of the split gate voltage V_{SG} is shown in Fig. 2b, from which we obtain a gate depletion value of $V_{SG} = 2.7$ V. At this point, the 1D channel is formed, and the total measured resistance is 5030 Ω. When indicated, this back gate-dependent series

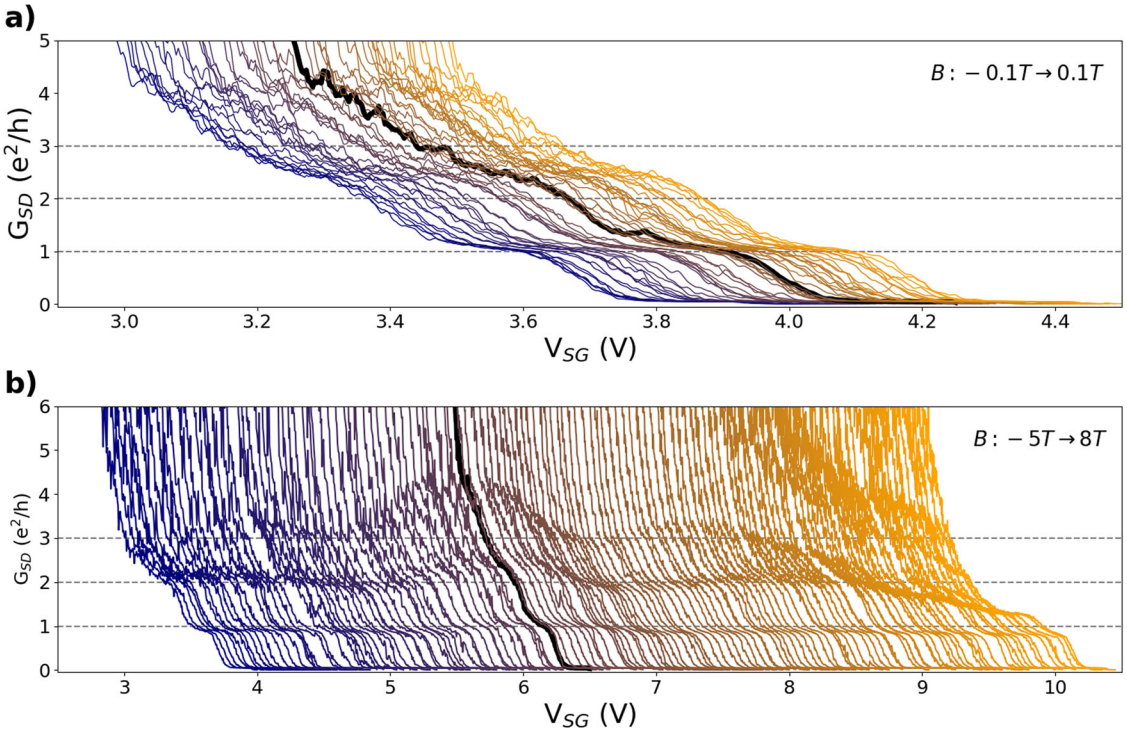

Fig. 3 Out-of-plane magnetic field $B_\perp$ dependence of the 1D channel. a Dependence of the quantized conductance plateaus on a perpendicular low magnetic field ranging from −100 to 100 mT and a resolution of 4 mT. **b** Dependence of the quantized conductance plateaus on a perpendicular magnetic field ranging from −5 to 8 T. In both panels, a horizontal offset is introduced between adjacent line traces for clarity. $V_{BG} = -33.2$ V for all runs with the corresponding lead resistance of $R_L = 5029\,\Omega$ subtracted.

resistance (see Supplementary Fig. 3) is subtracted from the raw data to obtain the conductance related only to the 1D channel[10]. In Fig. 2b, quantized conductance steps close to e^2/h and 2 e^2/h can be observed for a fixed hole concentration of 1.82×10^{12} cm^{-2} (see Supplementary Fig. 2). Tuning the concentration allows us to reach two different regimes, as demonstrated in Fig. 2c. At higher hole concentrations, below $V_{BG} = -30$ V, we see the appearance of the first conductance step at e^2/h. As the carrier concentration increases (V_{BG} decreases), the difference between the depletion and pinch-off values also increases and we observe the appearance of a second conductance step at a value of 2 e^2/h. These conductance steps are more clearly observed in a waterfall plot as shown in Fig. 2d. The observation of quantized conductance through the 600 nm long channel along with the high measured field-effect carrier mobility of $\mu_{FE} \approx 8000$–8500 cm^2 V^{-1} s^{-1}(see refs. [13,42,44,45]) (see Supplementary Fig. 2), hints toward quasi-ballistic transport and demonstrates that a high-quality monolayer WSe_2 sample has been achieved. At lower carrier concentrations, we observe the onset of a distinct transport regime that remains to be elucidated by further investigations (see Supplementary Fig. 7).

Magnetic field dependence of the 1D channel

We further investigate the quantized conductance features by applying a magnetic field perpendicular to the plane of the two-dimensional material. Due to the large hole spin and valley g-factor which has been reported to be up to 12 in monolayer WSe_2[46], we explore the low magnetic field regime between −100 and 100 mT (Fig. 3a) to eliminate any possible spin or valley polarization occurring due to a small magnetic field offset at 0 T. The quantization remains constant at low field even at a high resolution of 4 mT. We therefore conclude that the measured lifting of spin and valley degeneracies at low fields is inherent to this particular system leading to a ground state where only one conducting channel is available. At higher fields, as depicted in Fig. 3b, we observe that the first plateau remains constant between −5 and 8 T with a very small correction around 0 T which we attribute to magnetoresistance effects in the leads. This magnetoresistance correction is more significant at higher conductance, but after 1.5 T we observe the second and third quantization plateaus aligning with the values of 2 e^2/h and 3 e^2/h. This data set demonstrates that each conductance channel up to the third one allows transport for only one quantum of conductance. We cannot determine, however, what is the ground state in terms of spin or valley. In addition, at higher magnetic fields, we observe an evolution of the second and third plateaus in which they lower in conductance and seem to merge into the first plateau. No such change in conductance is observed for the first plateau. Measurements performed at 10 mK in a dilution refrigerator show the same behavior (see Supplementary Fig. 4).

Theory

In order to determine whether the anomalous quantization behavior originates from the spin-valley locking mechanism in TMDs, we developed a single-particle model of a 1D channel. To calculate single-hole states, we use a tight-binding model for WSe_2 monolayer[27,47–49] in a basis of three *d*-orbitals localized on tungsten atoms and three *p*-like orbitals describing Se_2 dimers (6 even orbitals in total). A single-particle channel wavefunction for a hole state *s* satisfies the Schrödinger equation[48,49]:

$$(H_{\text{bulk}} + |e|\phi)|\Psi^s\rangle = E^s|\Psi^s\rangle, \quad (1)$$

where the 1D electronic confinement defined within the WSe_2 monolayer lattice is determined by an applied gate-defined potential ϕ.

To obtain the channel potential landscape, we performed self-consistent Poisson–Schrödinger calculations[50,51] using parameters corresponding to the device used. The model includes the same

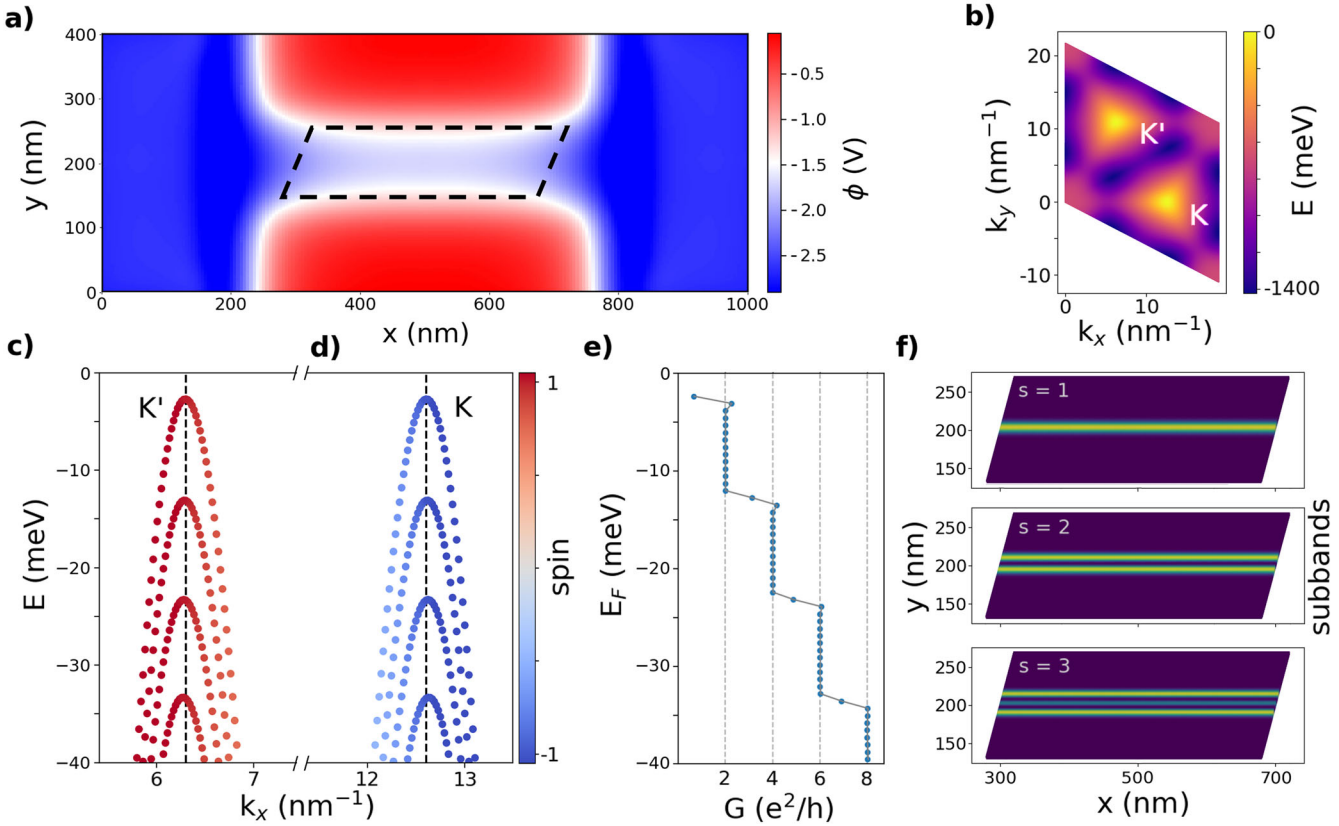

Fig. 4 Single-particle model of the 1D channel. a Potential profile from the Poisson–Schrödinger calculations. Within the WSe_2 monolayer (represented by computational rhombus -- dashed line), this profile forms a 1D gate-defined channel potential applied along the x axis. **b** Valence band energy surface within the Brillouin zone with two maxima at K' and K points. **c**, **d** Single-particle states calculated within the tight-binding model for WSe_2 monolayer rhombus with applied 1D gate-defined channel potential. The hole eigenstates, characterized by their energy, wave vector k_x, and spin, form characteristic parabolic subbands located in (**c**) K' valley with spin-up (red dots), or (**d**) K valley with spin-down (blue dots). Subsequent subbands are used to calculate the channel conductance (**e**) via the Landauer formula. Resulting conductance curve has a characteristic stepped-like shape with subsequent plateaus at multiples of 2 e^2/h. Those states (numbered by s quantum number) are occupied by hole states with spatial densities (**f**) resembling harmonic oscillator modes.

arrangement of layers represented by different dielectric constants and the same gate layout with the corresponding voltages applied. Further details can be found in the Supplementary Information. The obtained potential landscape results in a channel oriented along the x axis, and is presented together with an elongated rhombohedral tight-binding computational box that covers the channel area in Fig. 4a. A hole is free to move in the channel direction, while movement in the perpendicular direction is constrained by a Gaussian-like potential along the y axis. To simplify further calculations, we fit the channel profile at $x = 500$ nm with a Gaussian function ($U^{\mathrm{ch}} = U_0(1 - \exp(-\frac{y^2}{2\sigma^2}))$) resulting in a potential depth $U_0 = 1600$ mV and width $\sigma = 65$ nm. In the following calculations, we will use U^{ch} as a realistic approximation of the ϕ potential.

We define the finite tight-binding computational box in a form of a rhomboid of the WSe_2 lattice. We wrap the computational box on a torus, apply the periodic (Born-von Karman) boundary conditions, and obtain a set of allowed, discretized k-vectors over which we diagonalize the bulk Hamiltonian H_{bulk}. The valence band (VB) wavefunction for each allowed k-vector is a linear combination of Bloch functions on the W and Se_2 dimer sublattices $l (l = 1, \ldots, 6)$:

$$|\psi^{\mathrm{VB}}_{k\sigma}\rangle = \sum_{l=1}^{6} A^{\mathrm{VB}}_{k\sigma l} |\psi_{k,l}\rangle \otimes |\chi_\sigma\rangle, \tag{2}$$

where $|\chi_\sigma\rangle$ is the spinor part of the wavefunction, and

$$|\psi_{k,l}\rangle = \frac{1}{\sqrt{N}} \sum_{R_l=1}^{N} e^{i\mathbf{k}\cdot\mathbf{R}_l} \varphi_l(\mathbf{r} - \mathbf{R}_l) \tag{3}$$

are Bloch functions built with atomic orbitals φ_l. N is the number of unit cells, while $\mathbf{R}_l$ defines the position of atomic orbitals in the computational rhomboid. By diagonalising the 6 by 6 Hamiltonian H_{bulk} at each allowed value of k, we obtain the bulk energy bands $E^{\mathrm{VB}}_{k\sigma}$ and wavefunctions $A^{\mathrm{VB}}_{k\sigma l}$. The topmost valence band energy surface is shown in Fig. 4b, where two non-equivalent maxima, K and K' valleys, are clearly visible.

In the next step, we expand the channel wavefunction in terms of the lowest energy valence band states given by Eq. (2):

$$|\Psi^s_\sigma\rangle = \sum_k B^{\mathrm{VB},s}_{k\sigma} |\psi^{\mathrm{VB}}_{k\sigma}\rangle. \tag{4}$$

Finally, we solve the Schrödinger Eq. (1) with the potential term U^{ch} by converting it to an integral equation for the coefficients $B^{\mathrm{VB},s}_{k\sigma}$, and obtain the single-hole eigenstates confined within the channel,

$$E^{\mathrm{VB}}_{q\sigma} B^{\mathrm{VB},s}_{q\sigma} + \sum_k B^{\mathrm{VB},s}_{k\sigma} \sum_l \left(A^{\mathrm{VB}}_{q\sigma l}\right)^* A^{\mathrm{VB}}_{k\sigma l} |e| U^{\mathrm{ch}}_l(q,k) = E^s_\sigma B^{\mathrm{VB},s}_{q\sigma}, \tag{5}$$

where $U^{\mathrm{ch}}_l(q,k) = \frac{1}{N}\sum_{R_l=1}^{N} U^{\mathrm{ch}}(\mathbf{R}_l) e^{i(\mathbf{k}-\mathbf{q})\cdot\mathbf{R}_l}$ is the Fourier transform of the channel confinement on each sublattice l. The structural and the tight-binding Slater–Koster parameters in the calculations

are directly listed in the "Methods" section under tight-binding parameters.

The channel states of energy E_σ^s are characterized by subband index s, by the spin σ, and also by the valley K or K' determined by the expectation value of the wave vector $\langle k_x \rangle \equiv k_x$ in the channel direction. They belong to two different valleys: K' with spin-up—Fig. 4c, and K with spin-down—Fig. 4d, creating degenerate spin-valley locked states. Characteristic parabolic subbands are formed due to the lateral quantization within the channel represented by different values of s quantum number.

We note that the VB maximum (for the free hole Hamiltonian H_{bulk}) is shifted to zero and the highest energy state (ground state for holes in the channel) is located below, at −12 meV. The second spin-valley pair (not presented) is split-off by 0.5 eV below on the energy scale by the strong intrinsic spin-orbit coupling present in this material.

After calculating the single-particle eigenstates of the Hamiltonian H, we are ready to numerically estimate the conductance through the 1D channel. For each subband s, we calculate the density of states within the given subband $\frac{dN_s}{dE}$, and then estimate the particle velocity as $v_s(E) = \frac{1}{\hbar}\frac{\partial E_s}{\partial k_x}$. The conductance, which combines contributions from states from different occupied subbands s filled up to the Fermi energy, is calculated using the 2-terminal Landauer formula[52]:

$$G(E_F) = \frac{e^2}{E_F}\sum_s \int_0^{E_F} dE \frac{1}{2}\frac{dN_s}{dE} v_s(E). \quad (6)$$

The factor 1/2 is due to the fact that we take only states with $k_x > K_x$ (or $k_x > K'_x$ for the second valley), i.e., active under the given source-drain bias. In the above formula, we assume that no backscattering occurs. The calculated conductance is presented in Fig. 4e. It has the conductance plateaus at multiples of 2 e^2/h. The corresponding charge densities for each subband are plotted in Fig. 4f. The final result shows that a microscopic theory of a 1D channel predicts conductance steps in units of 2 e^2/h. Hence, we see that the measured e^2/h conductance quantization cannot be explained in the single-particle picture.

DISCUSSION

A possible explanation for the e^2/h conductance quantization can be obtained in terms of a broken symmetry valley-polarized ground state[25,26,39]. A valley-polarized state is expected to be the ground state of a 2D hole gas in a single layer of WSe_2 for sufficiently strong interaction strength and hole density (in analogy to WS_2[26]). The breaking of valley degeneracy naturally lifts the degeneracy of bands in the mean-field picture. Therefore, conductance plateaus in conductance quantization are expected to be half of the degenerate system, giving e^2/h instead of 2 e^2/h steps as a function of Fermi energy. This might explain the e^2/h plateau for a large range of hole densities, as shown in Fig. 2d.

In summary, we have fabricated high-quality monolayer WSe_2 devices where an electrostatically confined 1D hole transport channel is formed. At a temperature of 4 K, hole quasi-ballistic transport is observed, revealing an unexpected conductance quantization in steps of e^2/h instead of 2 e^2/h taking into account the electronic effects from the band structure of TMDs such as spin-valley locking. We have compared the experimental results to a single-particle atomistic tight-binding model for holes in WSe_2 with realistic channel profile and demonstrated that a 1D confining potential does not reproduce the measured conductance quantization in units of e^2/h. Recent experiments[25] and theory[27] suggest the existence of a valley-polarized state of the hole gas in TMDs. Such a state would explain the measured plateau at e^2/h. A theoretical model which includes hole–hole correlations is therefore necessary to explain quantum transport in 2D TMDs. These results show that the electronic properties of monolayer TMDs are still insufficiently understood and require further research to elucidate.

METHODS

Device fabrication

The device was assembled on a p-doped silicon substrate with 285 nm of thermally grown silicon dioxide (SiO_2). Using standard dry transfer methods[40,41], a flake of hexagonal boron nitride (hBN) (26 nm) was picked-up with a polypropylene carbonate (PPC) coated polydimethylsiloxane (PDMS) stamp and transferred onto lithographically patterned local gates. Electrical contacts [Cr (2 nm)/Pt (8 nm)][42] were subsequently patterned on top of the hBN. To remove any contaminants on the surface of the hBN and the electrical contacts, the sample was thermally annealed in a vacuum furnace (10^{-7} Torr) at 300 °C for 30 min and further cleaned mechanically using an atomic force microscope tip (AFM) in contact mode[8,22,53,54]. A second polymer stamp was used to subsequently pick-up an hBN flake (34 nm) then a monolayer WSe_2 flake. To ensure proper contact to the electrical contacts, the stack of flakes and stamp were placed in an AFM such that the surface of the WSe_2 flake was exposed where it was then mechanically cleaned using an AFM tip. The hBN/WSe_2 stack was then dropped off onto the patterned contacts. At this stage, the device was thermally annealed in a vacuum furnace following the same recipe as before. A final lithographic step was performed to pattern the top gates which include the two contact top gates (V_{CG}) and the split gates (V_{SG}).

Tight-binding parameters

In the tight-binding atomistic calculations, we chose the following structural parameters: $d_\parallel = 1.9188$ Å (W–Se_2 dimer center distance), $d_\perp = 1.6792$ Å (Se atom distance from $z = 0$ plane). The tight-binding Slater–Koster parameters are given by (all in eV): $E_d = -0.4330$, $E_{p0} = -3.8219$, $E_{p\pm1} = -2.3760$, $V_{dp\sigma} = -1.58193$, $V_{dp\pi} = 1.17505$, $V_{dd\sigma} = -0.90501$, $V_{dd\pi} = 1.0823$, $V_{dd\delta} = -0.1056$, $V_{pp\sigma} = 0.52091$, $V_{pp\pi} = -0.16775$, together with characterizing intrinsic spin-orbit couplings: $\lambda_W = 0.275, \lambda_{Se_2} = 0.08$. We note that these parameters are chosen to reproduce ab initio electronic band structure of two spinful valence bands.

DATA AVAILABILITY

The data that support the findings of this study are available from the corresponding author upon reasonable request.

Received: 4 October 2022; Accepted: 15 June 2023;
Published online: 15 July 2023

REFERENCES

1. Liu, X. & Hersam, M. C. 2D materials for quantum information science. *Nat. Rev. Mater.* **4**, 669–684 (2019).
2. Alfieri, A., Anantharaman, S. B., Zhang, H. & Jariwala, D. Nanomaterials for quantum information science and engineering. *Adv. Mater.* **35**, 2109621 (2022).
3. Zhang, Z.-Z. et al. Electrotunable artificial molecules based on van der Waals heterostructures. *Sci. Adv.* **3**, e1701699 (2017).
4. Pisoni, R. et al. Gate-tunable quantum dot in a high quality single layer MoS_2 van der Waals heterostructure. *Appl. Phys. Lett.* **112**, 123101 (2018).
5. Wang, K. et al. Electrical control of charged carriers and excitons in atomically thin materials. *Nat. Nanotechnol.* **13**, 128–132 (2018).
6. Krishnan, R., Biswas, S., Hsueh, Y.-L., Ma, H., Rahman, R. & Weber, B. Spin-valley locking for in-gap quantum dots in a MoS_2 transistor. *Nano Lett.* **23**, 6171–6177 (2023).
7. Davari, S. et al. Gate-defined accumulation-mode quantum dots in monolayer and bilayer WSe_2. *Phys. Rev. Appl.* **13**, 054058 (2020).
8. Boddison-Chouinard, J. et al. Gate-controlled quantum dots in monolayer WSe_2. *Appl. Phys. Lett.* **119**, 133104 (2021).

9. Pisoni, R. et al. Gate-defined one-dimensional channel and broken symmetry states in MoS_2 van der Waals heterostructures. *Nano Lett.* **17**, 5008–5011 (2017).
10. Marinov, K., Avsar, A., Watanabe, K., Taniguchi, T. & Kis, A. Resolving the spin splitting in the conduction band of monolayer MoS_2. *Nat. Commun.* **8**, 1938 (2017).
11. Epping, A. et al. Quantum transport through MoS_2 constrictions defined by photodoping. *J. Phys. Condens. Matter* **30**, 205001 (2018).
12. Lau, C. S. et al. Carrier control in 2D transition metal dichalcogenides with Al_2O_3 dielectric. *Sci. Rep.* **9**, 8769 (2019).
13. Sakanashi, K. et al. Signature of spin-resolved quantum point contact in p-type trilayer WSe_2 van der Waals heterostructure. *Nano Lett.* **21**, 7534–7541 (2021).
14. Field, M. et al. Measurements of Coulomb blockade with a noninvasive voltage probe. *Phys. Rev. Lett.* **70**, 1311 (1993).
15. Simmons, C. B. et al. Single-electron quantum dot in Si/SiGe with integrated charge sensing. *Appl. Phys. Lett.* **91**, 213103 (2007).
16. Güttinger, J. et al. Charge detection in graphene quantum dots. *Appl. Phys. Lett.* **93**, 212102 (2008).
17. Wang, L. et al. A graphene quantum dot with a single electron transistor as an integrated charge sensor. *Appl. Phys. Lett.* **97**, 262113 (2010).
18. Güttinger, J. et al. Time-resolved charge detection in graphene quantum dots. *Phys. Rev. B* **83**, 165445 (2011).
19. Volk, C. et al. Probing relaxation times in graphene quantum dots. *Nat. Commun.* **4**, 1753 (2013).
20. Fringes, S. et al. Charge detection in a bilayer graphene quantum dot. *Phys. Status Solidi B* **248**, 2684–2687 (2011).
21. Kurzmann, A. et al. Charge detection in gate-defined bilayer graphene quantum dots. *Nano Lett.* **19**, 5216–5221 (2019).
22. Boddison-Chouinard, J. et al. Charge detection using a van der Waals heterostructure based on monolayer WSe_2. *Phys. Rev. Appl.* **18**, 054017 (2022).
23. Thomas, K. J. et al. Possible spin polarization in a one-dimensional electron gas. *Phys. Rev. Lett.* **77**, 135–138 (1996).
24. Overweg, H. et al. Electrostatically induced quantum point contacts in bilayer graphene. *Nano Lett.* **18**, 553–559 (2017).
25. Scrace, T. et al. Magnetoluminescence and valley polarized state of a two-dimensional electron gas in WS_2 monolayers. *Nat. Nano.* **10**, 603–607 (2015).
26. Braz, Ja. E. H., Amorim, B. & Castro, E. V. Valley-polarized magnetic state in hole-doped monolayers of transition-metal dichalcogenides. *Phys. Rev. B* **98**, 161406 (2018).
27. Szulakowska, L., Cygorek, M., Bieniek, M. & Hawrylak, P. Valley- and spin-polarized broken-symmetry states of interacting electrons in gated MoS_2 quantum dots. *Phys. Rev. B* **102**, 245410 (2020).
28. Pawłowski, J., Bieniek, M. & Woźniak, T. Valley two-qubit system in a MoS_2-monolayer gated double quantum dot. *Phys. Rev. Appl.* **15**, 054025 (2021).
29. Thomas, K. J. et al. Possible spin polarization in a one-dimensional electron gas. *Phys. Rev. Lett.* **77**, 135–138 (1996).
30. Cronenwett, S. M. et al. Low-temperature fate of the 0.7 structure in a point contact: a Kondo-like correlated state in an open system. *Phys. Rev. Lett.* **88**, 226805 (2002).
31. Meir, Y., Hirose, K. & Wingreen, N. S. Kondo model for the "0.7 anomaly" in transport through a quantum point contact. *Phys. Rev. Lett.* **89**, 196802 (2002).
32. Rejec, T. & Meir, Y. Magnetic impurity formation in quantum point contacts. *Nature* **442**, 900–903 (2006).
33. Matveev, K. A. Conductance of a quantum wire in the Wigner-crystal regime. *Phys. Rev. Lett.* **92**, 106801 (2004).
34. Matveev, K. A. Conductance of a quantum wire at low electron density. *Phys. Rev. B* **70**, 245319 (2004).
35. Gücclü, A. D., Umrigar, C. J., Jiang, H. & Baranger, H. U. Localization in an inhomogeneous quantum wire. *Phys. Rev. B* **80**, 201302 (2009).
36. Welander, E., Yakimenko, I. I. & Berggren, K.-F. Localization of electrons and formation of two-dimensional Wigner spin lattices in a special cylindrical semiconductor stripe. *Phys. Rev. B* **82**, 073307 (2010).
37. Mehta, A. C., Umrigar, C. J., Meyer, J. S. & Baranger, H. U. Zigzag phase transition in quantum wires. *Phys. Rev. Lett.* **110**, 246802 (2013).
38. Micolich, A. P. What lurks below the last plateau: experimental studies of the $0.7 \times 2e^2/h$ conductance anomaly in one-dimensional systems. *J. Phys. Condens. Matter* **23**, 443201 (2011).
39. Van der Donck, M. & Peeters, F. M. Rich many-body phase diagram of electrons and holes in doped monolayer transition metal dichalcogenides. *Phys. Rev. B* **98**, 115432 (2018).
40. Wang, L. et al. One-dimensional electrical contact to a two-dimensional material. *Science* **342**, 614–617 (2013).
41. Boddison-Chouinard, J., Plumadore, R. & Luican-Mayer, A. Fabricating van der Waals heterostructures with precise rotational alignment. *J. Vis. Exp.* **149**, e59727 (2019).
42. Movva, H. C. P. et al. High-mobility holes in dual-gated WSe_2 field-effect transistors. *ACS Nano* **9**, 10402–10410 (2015).
43. Telford, E. J. et al. Via method for lithography free contact and preservation of 2D materials. *Nano Lett.* **18**, 1416–1420 (2018).
44. Jung, Y. et al. Transferred via contacts as a platform for ideal two-dimensional transistors. *Nat. Electron.* **2**, 187–194 (2019).
45. Chuang, H.-J. et al. High mobility WSe_2 p- and n-type field-effect transistors contacted by highly doped graphene for low-resistance contacts. *Nano Lett.* **14**, 3594–3601 (2014).
46. Gustafsson, M. V. et al. Ambipolar landau levels and strong band-selective carrier interactions in monolayer WSe_2. *Nat. Mater.* **17**, 411–415 (2018).
47. Bieniek, M. et al. Band nesting, massive Dirac fermions, and valley Landé and Zeeman effects in transition metal dichalcogenides: a tight-binding model. *Phys. Rev. B* **97**, 085153 (2018).
48. Bieniek, M., Szulakowska, L. & Hawrylak, P. Effect of valley, spin, and band nesting on the electronic properties of gated quantum dots in a single layer of transition metal dichalcogenides. *Phys. Rev. B* **101**, 035401 (2020).
49. Altıntaş, A. et al. Spin-valley qubits in gated quantum dots in a single layer of transition metal dichalcogenides. *Phys. Rev. B* **104**, 195412 (2021).
50. Pawłowski, J., Żebrowski, D. & Bednarek, S. Valley qubit in a gated MoS_2 monolayer quantum dot. *Phys. Rev. B* **97**, 155412 (2018).
51. Pawłowski, J., Szumniak, P. & Bednarek, S. Electron spin rotations induced by oscillating Rashba interaction in a quantum wire. *Phys. Rev. B* **93**, 045309 (2016).
52. Kouwenhoven, L. P., Schön, G. & Sohn, L. L. Introduction to Mesoscopic Electron Transport. In *Mesoscopic Electron Transport*, NATO ASI Series, Vol. 345 (eds Sohn, L. L., Kouwenhoven, L. P. & Schön, G.) 1–44 (Springer Netherlands, 1997).
53. Goossens, A. M. et al. Mechanical cleaning of graphene. *Appl. Phys. Lett.* **100**, 0003–6951 (2012).
54. Rosenberger, M. R. et al. Nano-"squeegee" for the creation of clean 2D material interfaces. *ACS Appl. Mater. Interfaces* **10**, 1944–8244 (2018).

ACKNOWLEDGEMENTS

We would like to thank Dr. Andrew Sachrajda for the fruitful discussions. This work was supported by the High Throughput and Secure Networks Challenge Program and the Quantum Sensors Challenge Program at the National Research Council of Canada. This research was supported by NSERC QC2DM Strategic Grant No. STPG-521420, NSERC Discovery Grant No. RGPIN- 2019-05714, and University of Ottawa Research Chair in Quantum Theory of Quantum Materials, Nanostructures, and Devices. J.P. acknowledges support from National Science Centre, Poland, under grant no. 2021/43/D/ST3/01989. M.B. acknowledges financial support from the Polish National Agency for Academic Exchange (NAWA), Poland, grant PPI/APM/2019/1/00085/U/00001. This research was enabled in part by support provided by the Digital Research Alliance of Canada (alliancecan.ca). This research was supported in part by PL-Grid Infrastructure.

AUTHOR CONTRIBUTIONS

J.B.-C., A.B., and L.G. designed the device architecture. J.B.-C., P.B., and J.L. fabricated the top gate structure, while J.B.-C. fabricated the remainder of the device with inputs from A.L.-M. and L.G. J.B.-C. performed the experimental measurements and the data analysis with consultations from A.B., A.L.-M., and L.G. Theoretical models and calculations were completed by J.P., D.M., M.B., and P.H. K.W. and T.T. grew the hexagonal boron nitride crystals. All authors participated in the writing of the manuscript.

COMPETING INTERESTS

The authors declare no competing interests.

ADDITIONAL INFORMATION

Supplementary information The online version contains supplementary material available at https://doi.org/10.1038/s41699-023-00407-y.

Correspondence and requests for materials should be addressed to Adina Luican-Mayer or Louis Gaudreau.